Featured in Physics

Atomic Compass: Detecting 3D Magnetic Field Alignment with Vector Vortex Light

Francesco Castellucci,[1,*] Thomas W. Clark,[2,*,†] Adam Selyem,[3] Jinwen Wang,[1,4] and Sonja Franke-Arnold[1,‡]
[1]School of Physics and Astronomy, University of Glasgow, Glasgow G12 8QQ, United Kingdom
[2]Wigner Research Centre for Physics, Budapest H-1525, Hungary
[3]Fraunhofer Centre for Applied Photonics, Glasgow G1 1RD, United Kingdom
[4]Shaanxi Province Key Laboratory of Quantum Information and Quantum Optoelectronic Devices, School of Physics, Xi'an Jiaotong University, Xi'an 710049, China

(Received 13 July 2021; accepted 7 October 2021; published 30 November 2021)

We describe and demonstrate how 3D magnetic field alignment can be inferred from single absorption images of an atomic cloud. While optically pumped magnetometers conventionally rely on temporal measurement of the Larmor precession of atomic dipoles, here a cold atomic vapor provides a spatial interface between vector light and external magnetic fields. Using a vector vortex beam, we inscribe structured atomic spin polarization in a cloud of cold rubidium atoms and record images of the resulting absorption patterns. The polar angle of an external magnetic field can then be deduced with spatial Fourier analysis. This effect presents an alternative concept for detecting magnetic vector fields and demonstrates, more generally, how introducing spatial phases between atomic energy levels can translate transient effects to the spatial domain.

DOI: 10.1103/PhysRevLett.127.233202

Most investigations and applications of light-atom interaction are concerned with homogeneously polarized light or scalar light. Light-atom interaction, however, by its very nature, is a vectorial process that depends explicitly on the alignment between an external magnetic field and the optical and atomic polarizations [1–6]. Over the last decades, the generation and use of vectorial light fields with spatially varying polarization profiles has matured into an active research area, with a plethora of applications in the optical domain [7–11], including communication [12], polarimetry [13], and superresolution imaging [14]. Our ability to design complex vector light fields now allows the full exploration of vectorial light-matter interaction [5]. One of the earliest examples is the prediction [15] and measurement [16] of the rotational Doppler effect, with more recent applications including complex image memories [17,18], manipulation of nonlinear effects [19,20], investigations of spatial anisotropy [21–23], and spatially dependent electromagnetically induced transparency [24–26].

Here, we investigate the role of external magnetic fields on the propagation of vectorial light fields through atomic gases and specifically demonstrate that the 3D alignment of a magnetic field can be deduced from a single absorption profile of a vector vortex beam. Atomic gases are optically active media with a highly sensitive external field response, making them ideal candidates for magnetometry [27–30]. Atomic magnetometers have been developed to detect magnetic gradients [31], multiple components of the magnetic vector field [32–37], or to compensate magnetic backgrounds in 3D [38]. Typically, optically pumped atomic magnetometers are based on observing the coherent Larmor precession of polarized atomic spins in a magnetic field, whereas vector magnetometers may employ radio-frequency modulation to map the vector components onto different harmonics.

In this Letter, we demonstrate a fundamentally different approach, replacing the *dynamic* detection of the spin precession with the *spatially resolved* detection of the atomic response to vector vortex light. We investigate the interaction of cold ^{87}Rb atoms with vector vortex beams on the D_2 (780 nm) $F = 1 \rightarrow F' = 0$ transition, as indicated in Fig. 1, and show that the spatial transmission profile of such light depends strongly on the 3D alignment of a static external magnetic field. By observing the atoms' absorption profile, and specifically, its Fourier decomposition, we can deduce the alignment of the magnetic field in three dimensions. Similar to other recent work [39,40], our technique requires only a single probe beam, thereby avoiding potential transverse dephasing effects. Unlike these previous schemes, the $F = 1 \rightarrow F' = 0$ configuration allows us to decouple the effect of 3D alignment from a modification of the magnetic field strength: demonstrating an atomic compass based on the absorption profile of a vector vortex beam.

Concept and theoretical model.—The interaction of atoms with light is, to first order, determined by the atomic dipole Hamiltonian

$$\hat{H} = -\mathbf{D} \cdot \mathbf{E} + g_F \mu_B \mathbf{F} \cdot \mathbf{B}, \tag{1}$$

where $\mathbf{E}$ and $\mathbf{B}$ are the electric vector field and the external static magnetic field, $\mathbf{D}$ and $\mathbf{F}$ are the induced atomic

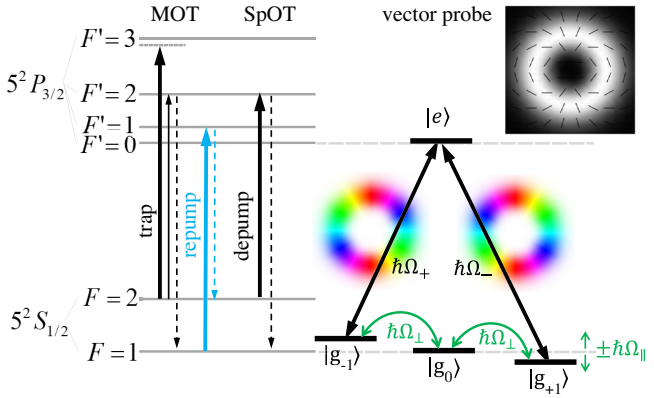

FIG. 1. Schematic energy levels and laser transitions: Rb^{87} atoms are cooled and trapped in a standard MOT and then transferred into a SpOT, populating the $F = 1$ ground state. A vector vortex beam drives a Λ transition, where the $\sigma_\pm$ transitions carry opposite phase profiles and an external magnetic field couples the ground states. The phase profiles of the probe light are shown for $\ell = \pm 2$, with hue representing values between 0 and 2π. The top inset shows the corresponding intensity and polarization profile.

electric dipole and atomic spin polarization, g_F is the Landé g factor, and μ_B is the Bohr magneton. In a closed system, an equilibrium can be reached, where the steady-state atomic system is polarized according to the optical polarization pattern, and the response of the optical field depends on the alignment of the optical polarization with respect to $\mathbf{B}$.

Circularly polarized light generates atomic dipole moments, causing optical dichroism, whereas linear polarization leads to atomic quadrupole moments, which generate birefringence [41]. A vector vortex beam

$$\mathbf{E}(\mathbf{r}) = \frac{1}{\sqrt{2}} E(r)[e^{-i\ell\phi}\hat{\boldsymbol{\sigma}}_+ + e^{i\ell\phi}\hat{\boldsymbol{\sigma}}_-] \tag{2}$$

represents the latter case. Here, the left and right circularly polarized components $\hat{\boldsymbol{\sigma}}_\pm$ carry equal and opposite orbital angular momentum $\mp\ell$, resulting in a polarization pattern, whose linear polarization rotates with the azimuth ϕ as shown in the inset of Fig. 1. Although such absolute phase effects are generally meaningless, a break in symmetry, e.g., due to an external magnetic field, can make the dependence measurable [24].

The inscribed structure of magnetic quadrupole moments generates locally varying birefringence, in turn modifying the propagation of the light through the atomic sample. The induced atomic alignment precesses around an applied magnetic field,

$$\mathbf{B}(\mathbf{r}) = B_0(\sin\theta_B\cos\phi_B\hat{\mathbf{x}} + \sin\theta_B\sin\phi_B\hat{\mathbf{y}} + \cos\theta_B\hat{\mathbf{z}}), \tag{3}$$

where θ_B and ϕ_B denote the inclination from the propagation axis and the azimuthal angle, respectively.

The atomic response is determined by the interplay between the local polarization direction of the light and the global external magnetic field. The spatial features of the resulting absorption profile can be analyzed in terms of their angular Fourier decomposition, allowing us to identify the 3D magnetic field alignment from a single absorption image.

We consider a standard Zeeman, Λ-type transition, resonantly coupling the $F = 1$, $m_F = \pm 1$ Zeeman sublevels, denoted as $|g_{\pm 1}\rangle$, to the $F' = 0$, $m'_F = 0$ excited state $|e\rangle$, as indicated in Fig. 1. The $F = 1$, $m_F = 0$ sublevel of the ground state, is denoted as $|g_0\rangle$. The transition is driven by weak vector vortex probe light (2) in the presence of a static magnetic field (3) with arbitrary inclination θ_B and azimuth ϕ_B.

The Hamiltonian in the Zeeman basis reveals a strong relationship between the geometry of the applied field and the energy of the system

$$\hat{H}_Z = \hbar\left[\pm\Omega_\parallel|g_{\pm1}\rangle\langle g_{\pm1}| - e^{\mp\phi_B}\frac{\Omega_\perp}{\sqrt{2}}|g_{\pm1}\rangle\langle 0| - \frac{\Omega_\pm}{2}|g_{\pm1}\rangle\langle e|\right] + \text{H.c.}, \tag{4}$$

where we have assumed resonant optical coupling. Here $\Omega_\pm = \exp(\mp i\ell\phi)\Omega_R/\sqrt{6}$ denotes the optical coupling, where Ω_R is the Rabi frequency, and we have considered the appropriate Wigner-Eckart coefficients. The effect of the magnetic field component along and orthogonal to the optical axis imposes a Zeeman shift on the states $|g_{\pm1}\rangle$ and mixing of the Zeeman sublevels, characterized by $\Omega_\parallel = \Omega_L\cos\theta_B$ and $\Omega_\perp = \Omega_L\sin\theta_B$, respectively, where $\Omega_L = g_F\mu_B B_0$ is the Larmor frequency.

The Hamiltonian can then be rewritten in terms of spatially dependent partially dressed states $|\psi_i\rangle$, such that

$$\hat{H}_\psi = \frac{\hbar}{2}\left[\Omega_L\cos\ell\phi\sin\theta_B|\psi_1\rangle\langle\psi_2| + \Omega_L N(\phi)|\psi_2\rangle\langle\psi_c| + \frac{\Omega_R}{2\sqrt{3}}|\psi_c\rangle\langle e|\right] + \text{H.c.} \tag{5}$$

The states $|\psi_i\rangle$ and the normalization factor $N(\phi)$ depend on ϕ, ϕ_B, and θ_B. See Supplemental Material for the relevant transformation and expressions [42]. In the spatially dependent basis, the structure in the optical coherence is now explicitly manifest in the magnetic interaction. In the absence of a magnetic field, $|\psi_1\rangle$ does not interact with the optical fields, being equivalent to the unperturbed ground state $|0\rangle$, but in the presence of a transverse magnetic field, there are certain values of ϕ for which the coherence still necessarily vanishes, i.e., for $\phi = n\pi/(2\ell)$ $\forall$ $n \in \mathbb{N}_0$, creating a magnetically induced, spatially dependent dark state, where there can be no absorption once the steady state is reached.

Using Fermi's golden rule (FGR), and so considering the cumulative probability that a photon will transition between $|\psi_1\rangle$ and $|\psi_c\rangle$, we obtain a concise insight into the analytical form of the interaction

$$T_{1\to e} \propto \Omega_L^4 \Omega_R^2 \sin^2\theta_B \cos^2(\ell\phi - \phi_B) \times [\cos^2\theta_B + \sin^2\theta_B \sin^2(\ell\phi - \phi_B)]. \quad (6)$$

Rewriting Eq. (6) as a cosine Fourier series, we can identify the azimuth ϕ_B and the inclination θ_B from the phase and magnitude of the Fourier components as

$$\phi_B = 2^{-1} \arg[\mathcal{F}_\phi(T_{1\to e})]_{2\ell}, \quad (7)$$

$$\sin^4\theta_B = \sqrt{8/\pi}|\mathcal{F}_\phi(T_{1\to e})|_{4\ell}, \quad (8)$$

forming the basis of what we might call a spatial atomic compass. The transition probability $T_{1\to e}$ and selected absorption profiles are shown in Fig. 2. Rotating **B** azimuthally results in a $1/\ell$-fold rotation of the absorption profile, whereas its inclination results in a splitting of the absorption pattern. The latter is reminiscent of the splitting of an absorption peak observed in [43]. We note that the magnetic field amplitude $|\vec{B}|$ enters Eq. (6) via the Larmor frequency as an overall scaling factor, affecting the overall fringe visibility of the absorption profile. This offers, as long as the perturbative limit holds, access to the field strength, in addition to its alignment.

We will show in the following that the analytic predictions based on FGR agree qualitatively with our experimental results. It fails, however, to describe some of the subtle atomic response, especially when dealing with **B** fields that are largely orthogonal to the optical propagation direction or for higher probe power. A rigorous treatment, based on optical Bloch equations [25,44,45], results in simulations that are in excellent quantitative agreement with our measurements, however, without permitting a simple analytical description. See the Supplemental Material for an overview [42].

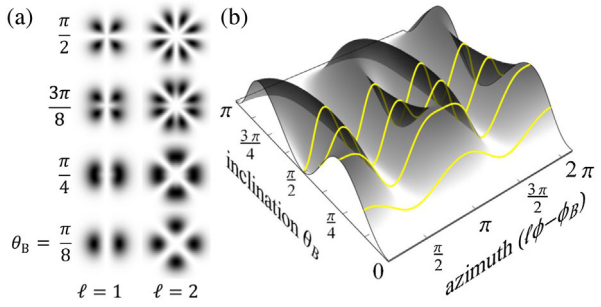

FIG. 2. Illustration of the transition probability $T_{1\to e}$ based on Fermi's golden rule. (a) Predicted absorption profiles for vector beams with $\ell = 1$ and 2 for the indicated inclination angles. (b) $T_{1\to e}$ as a function of the magnetic field alignment.

Experimental realization and discussion.—A cold atomic cloud, optical probe light, and global magnetic field **B** were created and combined in a simple linear arrangement (Fig. 3). For each alignment of **B**, the spatially dependent absorption profile, proportional to the optical density $\mathrm{OD} = \ln[(I_{\mathrm{probe}} - I_{\mathrm{back}})/(I_{\mathrm{trans}} - I_{\mathrm{back}})]$, was recorded and the consequent Fourier components extracted, where I_{probe}, I_{trans}, and I_{back} represent the intensity of the probe before and after absorption and the background intensity, respectively, with examples shown in Fig. 4(a). The atomic cloud was formed from ^{87}Rb atoms collected in a magneto-optical trap (MOT), before transfer to the $F = 1$ ground state of a dark spontaneous-force optical trap (SpOT) [46] (Fig. 1). Approximately 5×10^7 atoms were evenly distributed over the three Zeeman sublevels, while maintaining an atomic density of 10^{11} cm^{-3} and a temperature of 100 μK. The trapping, repump, and depump beams, as well as the MOT's magnetic quadrupole field, were then switched off and the cloud expanded freely for 3.5 ms before interaction with the vector vortex probe light. Such light, locked to the $F = 1 \to F' = 0$ transition, was generated with a q plate [47], where the measured polarization and intensity profile is shown in Fig. 4(a) for $\ell = 2$. The probe power was varied over a range from 0.03 to 0.5 μW, but had greatest agreement with Eq. (6) for lower values, corresponding to a perturbative regime. The results presented in Fig. 4 were taken with a total beam power of 0.13 μW, corresponding to a Rabi frequency of $\Omega_R = 2\pi \times 0.26$ MHz in the region of interest, indicated by the red lines in Fig. 4(a).

Before interaction, a global **B** field with a fixed magnitude was generated and applied using three orthogonal sets of rectangular coils, varying ϕ_B and θ_B in steps of 80 mrad for each run. All data shown in this Letter were obtained for 1×10^{-4} T, but analogous results were confirmed for fields between 0.5 and 3×10^{-4} T. Following standard practice, the desired external field **B** was added to a cancellation field, already applied during the operation of the MOT and SpOT, and opposing any spurious environmental fields at the position of the atomic cloud.

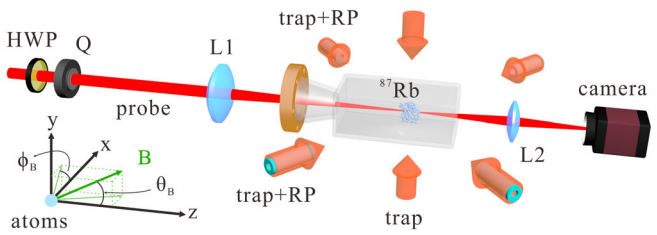

FIG. 3. Schematic diagram of the experimental geometry. The atoms are in the far field of the q plate (Q) and are imaged to the camera plane. The optical pumping configuration for the SpOT is explained in [46]. The bottom left inset shows the defining coordinate system and the alignment of the magnetic field. HWP, half wave plate; L, lens; RP, repump.

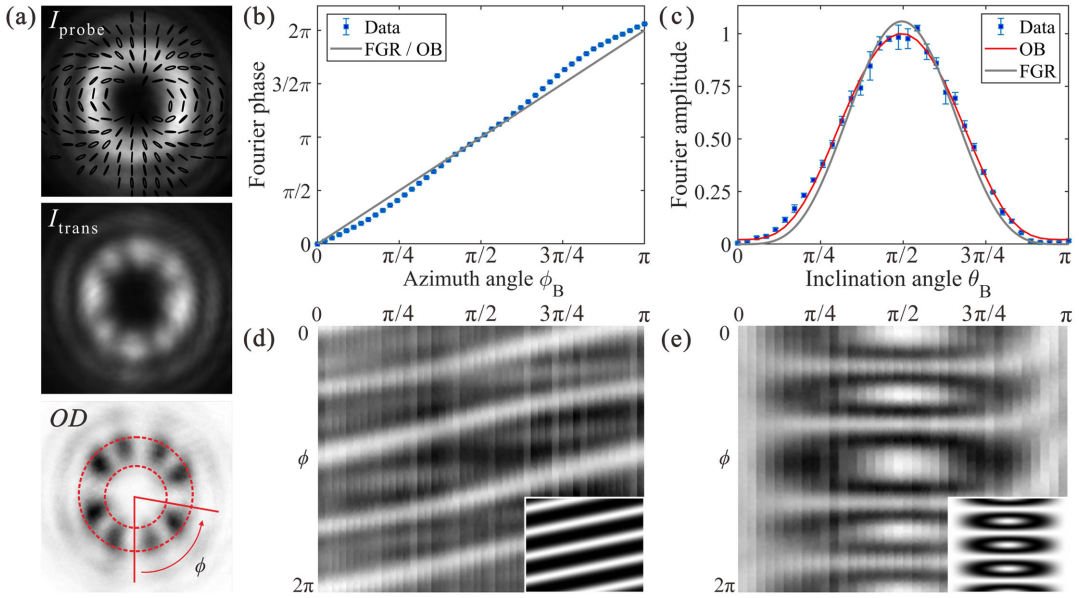

FIG. 4. Magnetic field alignment from Fourier analysis of the atomic absorption profiles. (a) Example images ($600 \times 600\ \mu m^2$) in gray scale of the probe intensity I_{probe}, transmitted light I_{trans}, and resulting transmission profile OD (where black corresponds to high OD), with the analysis region indicated in red. (b),(c) Dependence of the 2ℓ and 4ℓ Fourier components on ϕ_B and θ_B of the **B** and comparison with FGR and optical Bloch model (OB). Error bars of the data points (blue) represent the standard deviation of 3 or 5 runs. (d),(e) Corresponding compilations of the unwrapped OD images for steps of 70 and 87 mrad, respectively, with the FGR prediction as insets.

Qualitatively, the results confirm that the absorption pattern rotates azimuthally with applied **B**, Fig. 4(d), and splits from 2ℓ to 4ℓ lobes when its inclination from the optical axis rises from 0 to $\pi/2$, Fig. 4(e). The quantitative comparisons, based on Fourier analysis of the data and models, are presented in Figs. 4(b) and 4(c). The analytical predictions of Eqs. (7) and (8), shown as gray lines, are largely in agreement with the data. In our experiment, we had to balance the low probe intensity required for the weak-coupling limit with the necessity for high contrast absorption images from our detectors. Therefore, although providing a concise insight, the perturbative regime required for Eq. (6) was not fully applicable to our conditions, and we may observe a spatial analog of intensity broadening. A model based on the full optical Bloch equations, normalized to the data and fitting on the beam intensity, leads to excellent agreement.

The remaining discrepancies in the data are likely technical in origin. The polarization profile of our probe shows small (ϕ-dependent) degrees of ellipticity, corresponding to an imbalance between the $\sigma_\pm$ light components. Furthermore, we are using the magnetic field cancellation coils of a standard MOT setup to define our **B** alignment, and any incomplete cancellation of environmental fields may result in a small tilt from the desired alignment, providing a likely source of systematic experimental uncertainty. Random error, however, was reduced to acceptable levels, as indicated by standard deviations, averaging over five and three runs for each θ_B and ϕ_B, respectively [Figs. 4(b) and 4(c)]. The corresponding precision of the **B** field alignment, after inverting Eqs. (7) and (8), was 30 mrad for both ϕ_B and θ_B.

We note that the emphasis of this Letter is on the fundamental concept of measuring magnetic field alignment via spatial, rather than time-resolved detection. Our experiment is neither optimized nor competitive in terms of sensitivity. On a fundamental level, the highest possible sensitivities for optical atomic magnetometers, realized, e.g., in spin-exchange relaxation-free and radio-frequency magnetometers, are obtained by minimizing spin-relaxation rates. The same mechanism applies also to our technique: spin alignment is established at a rate given by the Larmor frequency and destroyed due to collisions among the cold atoms. For our parameters, we expect a collision rate that should allow the detection of **B** fields of about 50 pT.

Conclusions.—Throughout, we exposed a spatial relationship between magnetic field alignment and phase-shaped light on interaction with an atomic cloud. Using this relationship, we have shown, analytically and experimentally, how an atomic cloud may be used as a three-dimensional compass, without explicitly invoking time-dependent effects. The 3D alignment is derived from individual absorption images obtained in single-axis optical probing, where a vector vortex probe beam both generates and measures the atomic polarization. These results hold in the steady-state limit and can be largely independent of applied field strength, offering opportunities for a new

branch of magnetic sensing. This parallel geometry is promising for the development of chip-based and miniature sensors. In principle, the effect also holds for warm vapors, with the caveat that transitions $F = 1 \rightarrow F' = 0$ would, due to Doppler broadening, also excite $F' = 1$ and 2, which in combination with thermal motion would reduce the signal.

Although our present demonstration uses a simple vector vortex beam to detect homogeneous magnetic fields, the principle may be generalized to arbitrary vector light fields, with possible applications to inertial, gradient, and position sensing and long term magnetic effects, as well as magnetic anomaly detection. In our current setup, we use azimuthal polarization patterns and deduce the magnetic field alignment from an angular Fourier analysis of the measured optical density. As this method does not rely on the radial degree of freedom, we could detect a radially varying field alignment. Instead, optical beams with linear polarization modulation could be generated from superpositions of Hermite-Gaussian modes, which would lend themselves to the analysis of linear changes in $\mathbf{B}$.

This spatial mapping to a magnetic field can be quite general, providing an original toolkit for the spatial manipulation of magnetic dipole and quadrupole moments in atoms. With asymmetric polarization patterns, we not only expect greater field information in the absorption patterns, but we would also obtain programmable dispersion relations, where early results suggest practical gains in magneto-optical rotation, as well as fundamental insight into spatial analogs of the Kramers-Kronig relations.

The data set for this paper is available from Ref. [48].

The authors would like to thank Péter Domokos for supporting the collaboration and Gergely Szirmai for stimulating discussions regarding Fourier transforms in unusual bases. F. C. and S. F.-A. acknowledge financial support from the European Training Network ColOpt, funded by the European Union Horizon 2020 program under the Marie Sklodowska-Curie Action, Grant Agreement No. 721465. T. W. C. acknowledges support by the National Research, Development, and Innovation Office of Hungary (NKFIH) within the Quantum Technology National Excellence Program (Project No. 2017-1.2.1-NKP-2017-00001). J. W. acknowledges support by the China Scholarship Council (CSC) (No. 201906280228).

*These authors contributed equally to this work.
†thomas.clark@wigner.hu
‡sonja.franke-arnold@glasgow.ac.uk

[1] D. Budker, W. Gawlik, D. Kimball, S. Rochester, V. Yashchuk, and A. Weis, Rev. Mod. Phys. **74**, 1153 (2002).
[2] S. Franke-Arnold, Phil. Trans. R. Soc. A **375**, 20150435 (2017).
[3] G. Labeyrie, I. Krešić, G. R. M. Robb, G.-L. Oppo, R. Kaiser, and T. Ackemann, Optica **5**, 1322 (2018).
[4] M. Babiker, D. L. Andrews, and V. E. Lembessis, J. Opt. **21**, 013001 (2019).
[5] J. Wang, F. Castellucci, and S. Franke-Arnold, AVS Quantum Sci. **2**, 031702 (2020).
[6] T. Ackemann, G. Labeyrie, G. Baio, I. Krešić, J. G. M. Walker, A. C. Boquete, P. Griffin, W. J. Firth, R. Kaiser, G.-L. Oppo, and G. R. M. Robb, Atoms **9**, 35 (2021).
[7] Q. Zhan, Adv. Opt. Photonics **1**, 1 (2009).
[8] H. Rubinsztein-Dunlop, A. Forbes, M. V. Berry, M. R. Dennis, D. L. Andrews, M. Mansuripur, C. Denz, C. Alpmann, P. Banzer, T. Bauer *et al.*, J. Opt. **19**, 013001 (2017).
[9] C. Rosales-Guzmán, B. Ndagano, and A. Forbes, J. Opt. **20**, 123001 (2018).
[10] J. Chen, C. Wan, and Q. Zhan, Sci. Bull. **63**, 54 (2018).
[11] A. Forbes and I. Nape, AVS Quantum Sci. **1**, 011701 (2019).
[12] B. Ndagano, I. Nape, M. A. Cox, C. Rosales-Guzman, and A. Forbes, J. Lightwave Technol. **36**, 292 (2017).
[13] R. D. Hawley, J. Cork, N. Radwell, and S. Franke-Arnold, Sci. Rep. **9**, 2688 (2019).
[14] R. Dorn, S. Quabis, and G. Leuchs, Phys. Rev. Lett. **91**, 233901 (2003).
[15] L. Allen, M. Babiker, and W. Power, Opt. Commun. **112**, 141 (1994).
[16] S. Barreiro, J. W. R. Tabosa, H. Failache, and A. Lezama, Phys. Rev. Lett. **97**, 113601 (2006).
[17] V. Parigi, V. D'Ambrosio, C. Arnold, L. Marrucci, F. Sciarrino, and J. Laurat, Nat. Commun. **6**, 7706 (2015).
[18] Y.-H. Ye, M.-X. Dong, Y.-C. Yu, D.-S. Ding, and B.-S. Shi, Opt. Lett. **44**, 1528 (2019).
[19] F. Bouchard, H. Larocque, A. M. Yao, C. Travis, I. De Leon, A. Rubano, E. Karimi, G.-L. Oppo, and R. W. Boyd, Phys. Rev. Lett. **117**, 233903 (2016).
[20] H. Hu, D. Luo, and H. Chen, Appl. Phys. Lett. **115**, 211101 (2019).
[21] F. K. Fatemi, Opt. Express **19**, 25143 (2011).
[22] J. Wang, X. Yang, Y. Li, Y. Chen, M. Cao, D. Wei, and H. Gao, and F. Li, Photonics Res. **6**, 451 (2018).
[23] J. Wang, X. Yang, Z. Dou, S. Qiu, J. Liu, Y. Chen, M. Cao, H. Chen, D. Wei, K. Müller-Dethlefs *et al.*, Appl. Phys. Lett. **115**, 221101 (2019).
[24] N. Radwell, T. W. Clark, B. Piccirillo, S. M. Barnett, and S. Franke-Arnold, Phys. Rev. Lett. **114**, 123603 (2015).
[25] H. R. Hamedi, V. Kudriašov, J. Ruseckas, and G. Juzeliūnas, Opt. Express **26**, 28249 (2018).
[26] X. Yang, Y. Chen, J. Wang, Z. Dou, M. Cao, D. Wei, H. Batelaan, H. Gao, and F. Li, Opt. Lett. **44**, 2911 (2019).
[27] D. Budker, D. F. Kimball, S. M. Rochester, V. V. Yashchuk, and M. Zolotorev, Phys. Rev. A **62**, 043403 (2000).
[28] I. Kominis, T. Kornack, J. Allred, and M. V. Romalis, Nature (London) **422**, 596 (2003).
[29] D. Budker and M. Romalis, Nat. Phys. **3**, 227 (2007).
[30] R. S. Grewal, G. Pati, and R. Tripathi, Phys. Rev. A **102**, 033102 (2020).
[31] C. Affolderbach, M. Stähler, S. Knappe, and R. Wynands, Appl. Phys. B **75**, 605 (2002).

[32] V. I. Yudin, A. V. Taichenachev, Y. O. Dudin, V. L. Velichansky, A. S. Zibrov, and S. A. Zibrov, Phys. Rev. A **82**, 033807 (2010).
[33] B. Patton, E. Zhivun, D. C. Hovde, and D. Budker, Phys. Rev. Lett. **113**, 013001 (2014).
[34] L. Lenci, A. Auyuanet, S. Barreiro, P. Valente, A. Lezama, and H. Failache, Phys. Rev. A **89**, 043836 (2014).
[35] T. Thiele, Y. Lin, M. O. Brown, and C. A. Regal, Phys. Rev. Lett. **121**, 153202 (2018).
[36] S. J. Ingleby, C. O'Dwyer, P. F. Griffin, A. S. Arnold, and E. Riis, Phys. Rev. Applied **10**, 034035 (2018).
[37] T. Pyragius, H. M. Florez, and T. Fernholz, Phys. Rev. A **100**, 023416 (2019).
[38] A. Smith, B. E. Anderson, S. Chaudhury, and P. S. Jessen, J. Phys. B **44**, 205002 (2011).
[39] B. Chen, X. Hou, F. Ge, X. Zhang, Y. Ji, H. Li, P. Qian, Y. Wang, N. Xu, and J. Du, Nano Lett. **20**, 8267 (2020).
[40] S. Qiu, J. Wang, F. Castellucci, M. Cao, S. Zhang, T. W. Clark, S. Franke-Arnold, H. Gao, and F. Li, arXiv:2109.14405.
[41] M. Auzinsh, D. Budker, and S. Rochester, *Optically Polarized Atoms: Understanding Light-Atom Interactions* (Oxford University Press, New York, 2010).
[42] See Supplemental Material at http://link.aps.org/supplemental/10.1103/PhysRevLett.127.233202 for more details on state transformations and underlying models.
[43] L. Margalit, M. Rosenbluh, and A. D. Wilson-Gordon, Phys. Rev. A **87**, 033808 (2013).
[44] T. W. Clark, Sculpting shadows: On the spatial structuring of fields & atoms: A tale of light and darkness, Ph.D. thesis, University of Glasgow, 2016.
[45] S. Sharma and T. N. Dey, Phys. Rev. A **96**, 033811 (2017).
[46] N. Radwell, G. Walker, and S. Franke-Arnold, Phys. Rev. A **88**, 043409 (2013).
[47] L. Marrucci, C. Manzo, and D. Paparo, Phys. Rev. Lett. **96**, 163905 (2006).
[48] https://doi.org/10.5525/gla.researchdata.1203.